Structural Changes for π-Radicals of Free-Base Tetraphenylbacteriochlorin: A Model for the Electron Donor and Acceptor in Bacterial Reaction Centers

Ching-Yao Lin, Milton E. Blackwood, Jr., Ranjit Kumble, Songzhou Hu, and Thomas G. Spiro*

Department of Chemistry, Princeton University, Princeton, New Jersey 08544

Received: November 26, 1996; In Final Form: January 30, 1997[⊗]

Resonance Raman spectra are reported for electrochemically generated radical cations and anions of tetraphenylbacteriochlorin free-base, H_2TPBC, and also for the photogenerated triplet state T_1. Isotope substitution, including ^{13}C at the *meso* positions, and deuteration of the pyrrole or phenyl rings permit mode assignments and correlations with the ground state RR spectrum of H_2TPBC, for which a normal coordinate analysis has been carried out. Both up- and down-shifts of skeletal mode frequencies are observed. These shifts are satisfactorily calculated for the radical cation and anion by altering the stretching force constants of bonds in the conjugated π−system of bacteriochlorin. The force constant changes are in qualitative accord with expected bonding changes upon removing an electron from the HOMO or adding an electron to the LUMO. However the frequency changes in the T_1 state are much larger than expected from these bonding changes and are not reproduced by averaging the radical cation and anion force constants. Thus the T_1 molecular distortion is not simply related to the properties of the HOMO or LUMO.

Introduction

The bacteriochlorophyll chromophore has multiple functions in bacterial photosynthesis, harvesting light, and mediating the transfer of photoelectrons.[1] Photoexcitation of the light-harvesting complex produces energy transfer to the reaction center, where charge is separated, producing radical cations and anions.[2,3] The electronic and molecular structure of these radicals and of the photoexcited states are of interest and have been probed by a variety of spectroscopies. Among these, resonance Raman, RR, spectroscopy is capable of providing details of structural change via the normal mode energies and compositions.[4−9]

Interpretation of the spectra requires an understanding of the normal modes. We have recently reported a normal mode analysis of a model chromophore (Figure 1), tetraphenylbacteriochlorin free base, H_2TPBC, based on variable wavelength RR spectroscopy and isotopic substitution.[10] We now report RR spectra of the radical cation and anion of H_2TPBC and of its T_1 excited state. The richly detailed spectra have been correlated with the ground state spectra via correspondences in the isotopic shifts. We observe changes in the mode frequencies, both positive and negative, and have analyzed these changes with the aid of the H_2TPBC force field. Required force constant changes are in good qualitative accord with the bond-order changes expected upon removal of an electron from the HOMO, in the case of the radical cation, and addition of an electron to the LUMO, in the case of the radical anion.

However, the frequency changes observed in the T_1 RR spectra are much larger than the sum of the cation and anion frequency changes, even though formation of the triplet state involves the transfer of an electron from the HOMO to the LUMO. Additional structural changes are evidently involved in the triplet excitation. The available data show that this effect is not limited to bacteriochlorin. In porphyrins and in chlorins as well, the T_1 frequencies are not predictable on the basis of the radical cations and anions. The structural changes exceed the bonding changes associated with one-electron transfer in all the tetrapyrrole chromophore triplet states that have been examined so far.

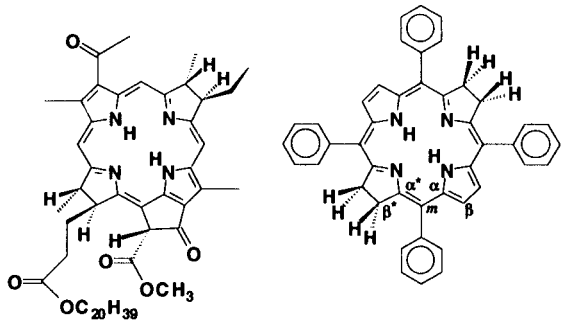

Figure 1. Molecular structure of bacteriopheophytin and free-base tetraphenylbacteriochlorin, along with the labeling scheme for the latter.

Experimental Section

Synthesis. H_2TPBC was prepared from free-base tetraphenylporphine (H_2TPP, Mid-Century, Posen, IL) according to the methods of Whitlock *et al.*[11] However, we found that using excess reducing agent (3 g of toluenesulfonylhydrazine to 200 mg of H_2TPP) dramatically shortened the reaction time from the reported 6.5 h to less than half an hour.

Free-base β-d_8-, *meso*-$^{13}C_4$-, and phenyl-d_{20}-TPBC were obtained from the respective porphyrin isotopomers, which were prepared from isotope-labeled pyrroles (d_5) and benzaldehydes (d_5 and ^{13}C) according to the method of Lindsey *et al.*[12] Deuterated H_2TPBCs (d_8 and d_{20}) were checked by NMR spectroscopy to ensure the quality of isotope labeling.

Electrochemistry and Spectroelectrochemistry. Cyclic voltammetry (CV) was performed with a three-electrode cell. A glassy carbon electrode (GCE), a saturated calomel electrode (SCE), and a platinum wire were used as working, reference,

* To whom correspondence should be addressed.
[⊗] Abstract published in *Advance ACS Abstracts,* March 15, 1997.

S1089-5647(96)03923-5 CCC: $14.00

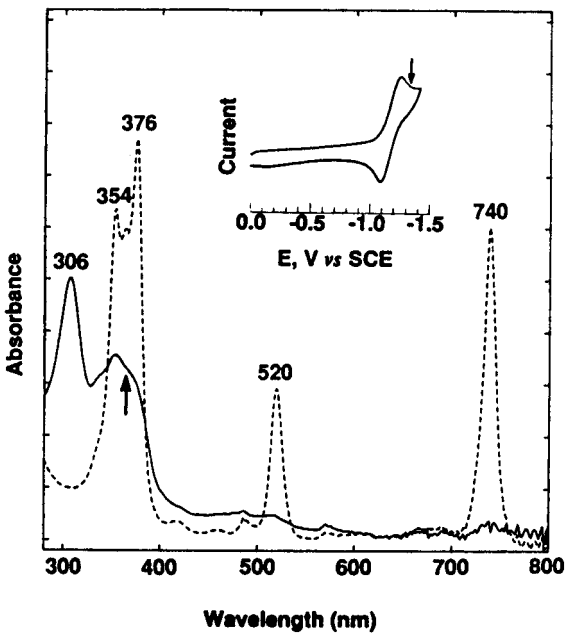

Figure 2. Absorption spectra for neutral H_2TPBC (dotted line) and its anion radical (solid line). The arrow indicates the excitation line used to record RR spectra for the anion radical. Inset: CV for H_2-TPBC reduction. The arrow indicates the applied potential used for thin-layer electrolysis. Conditions: THF with TBAP as electrolyte, $E_{applied} = -1.35$ V *vs* SCE, scan rate for the CV= 100 mV/s.

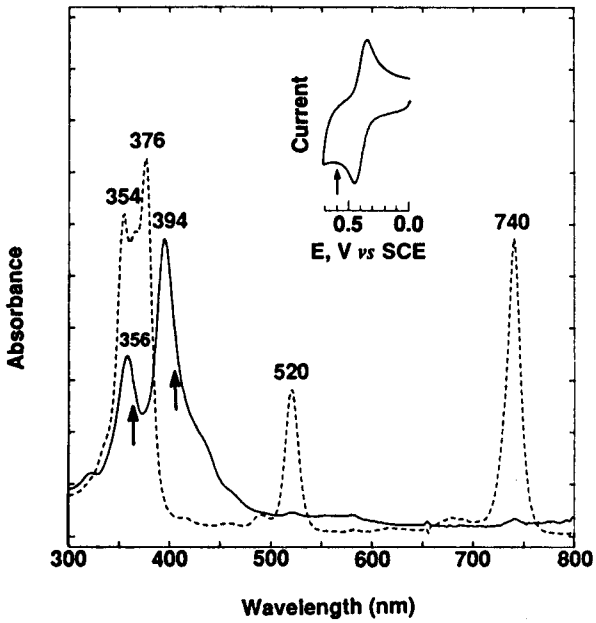

Figure 3. Same as Figure 3, but in CH_2Cl_2/TBAP for the cation radical. $E_{applied} = 0.6$ V *vs* SCE.

and counter electrode, respectively. Reference and counter electrodes were isolated from the main compartment either by a junction with a platinum wire on the tip or by a fine glass frit. Cyclic voltammograms were obtained with a Bioanalytical System Model BAS CV-27 potentiostat and an X−Y recorder. For controlled-potential electrolysis, a Princeton Applied Research potentiostat (Model 173) was used.

UV−vis spectroelectrochemistry was performed with an airtight, optically transparent thin-layer electrochemical (OTTLE) cell constructed with a 100 mesh platinum gauze working electrode in a 1 mm quartz cell (Figure 2). The OTTLE cell was equipped with an optically transparent vacuum dewar in order to carry out low-temperature experiments. Ultraviolet and visible spectra were recorded with a Hewlett-Packard diode array 8451A UV−vis spectrophotometer. The bulk electrolysis cell for resonance Raman experiments has been described previously.[13] Both electrolysis cells were assembled under an inert atmosphere in a glovebox to exclude moisture and oxygen.

Resonance Raman spectra were obtained in backscattering geometry from either THF or CH_2Cl_2 solution in a spinning NMR tube for the neutral species. Excitation lines were provided with a Coherent Innova 100K3 krypton ion laser (406.7 nm) and a Spectra-Physics 2025 argon ion laser (363.8 nm). The scattered light was collected and dispersed with a Spex 1877 triple monochromator equipped with a cooled intensified diode array detection system (Princeton Instruments). To minimize laser-induced degradation, solutions were prepared with freshly distilled THF or CH_2Cl_2, which were vigorously degassed with at least three freeze−pump−thaw cycles.

Time-Resolved Spectroscopy. All time-resolved experiments were performed in THF. The transient absorption spectrum of the T_1 state was obtained by measuring the change in absorption spectrum with a gated dual-diode array detector (Princeton Instruments) 100 ns after photoexcitation with a 532 nm pump pulse from a 10 Hz Q-switched Nd:YAG laser (Quanta Ray). The experimental setup is described in more detail elsewhere.[14] For the time-resolved resonance Raman (TR^3) experiments, a 532 nm pump pulse was again used along with a 397 nm probe pulse generated by Raman-shifting (first Stokes-shifted line of D_2) the third harmonic of the Nd:YAG laser. The probe pulse was sent down an optical delay path to arrive at the sample 25 ns after the pump pulse. Longer time delays were introduced with two synchronized Nd:YAG lasers to ensure that the reported spectra were not contaminated by singlet excited state features. A dichroic beamsplitter was utilized to spatially superimpose the pump and probe pulses, and a cylindrical lens was used to focus the beam onto the sample contained in an airtight 1 mm path length quartz cuvette. Scattered light was collected at 135° and dispersed in a triple-stage spectrograph equipped with an OMA detector (Princeton Instruments). A series of probe-only and pump/probe spectra were taken, and the exited state spectra were obtained by subtracting the summed probe-only spectra from the summed pump/probe spectra. Summed probe-only spectra (not shown) were compared with spectra obtained at 363.8 nm excitation (Figure 4) to ensure that the pulsed laser probe beam was not producing excited state features in the ground state spectra. The solvent features were removed from all reported spectra by subtraction of the Raman spectrum of pure THF.

All the spectral data were imported into and processed with Labcalc software (Galactic Industries Co., Salem, NH).

Normal Coordinate Analysis (NCA). Normal mode calculations were performed with the empirical **GF** matrix method of Wilson.[15] The molecular geometry was taken from the crystal structure of five-coordinated zinc tetraphenylbacteriochlorin[16] and slightly modified to retain D_{2h} symmetry. The internal coordinates are Wilson-type bond-stretching and angle-bending coordinates. The symmetry coordinates ($\mathbf{S}_i$) and the corresponding **U** matrix were obtained from a symmetry-adapted linear combination of internal coordinates. A menu-driven, graphically interfaced version of Schachtschneider's program,[17] developed in our laboratory and implemented on a R3000 Indigo workstation (Silicon Graphics Inc.), was used to set up the **G** matrix and to solve the secular equation $|\mathbf{GF} - \mathbf{E}\lambda| = 0$.

Results and Discussion

Electrochemistry and (UV−Vis) Spectroelectrochemistry. H_2TPBC undergoes reversible one-electron redox reactions; it is reduced to the anion radical at −1.15 V vs SCE in THF with

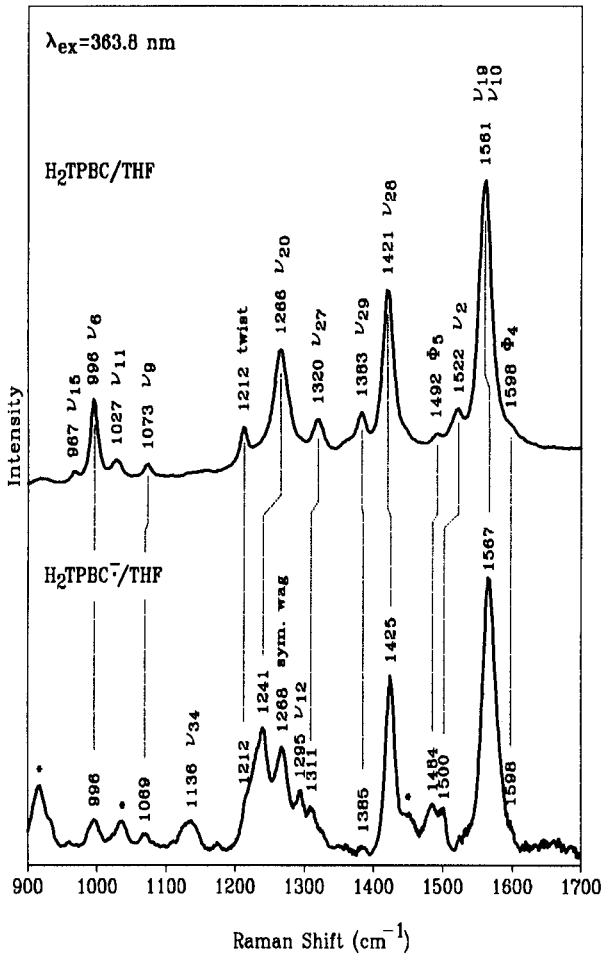

Figure 4. Soret-excited RR spectra of H_2TPBC and H2TPBC$^-$ in THF/TBAP. Asterisks indicate Raman bands of the solvent and the electrolyte. Conditions: 363.8 nm excitation, 50 mW, 4 cm^{-1} slit width.

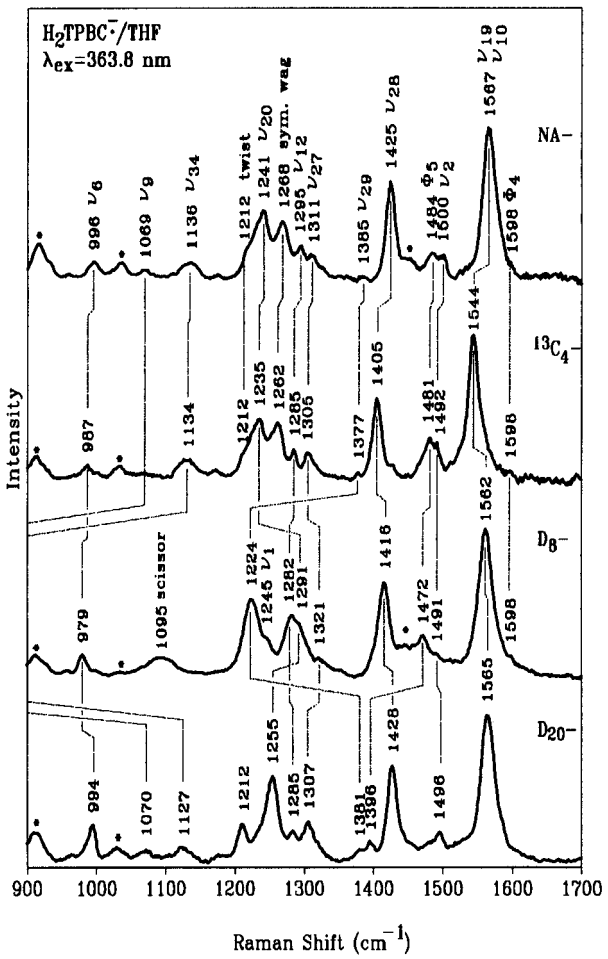

Figure 5. RR spectra for natural abundance (NA-), $^{13}C_4$-, -d_8, and -d_{20} H_2TPBC^-.

0.1 M electrolyte (TBAP) and oxidized to its radical cation at +0.42 V in CH_2Cl_2 (Figures 2 and 3, insets). These electrochemical characteristics are similar to previous reports.[18] The absorption spectral changes are also reversible upon one-electron reduction or oxidation. Upon reduction to the anion radical, the Soret bands of H_2TPBC shift from 376 and 354 nm to ~354 and 306 nm and the Q bands are bleached (Figure 2). Oxidation to the cation radical shifts the Soret bands to 394 and 356 nm, and replaces the Q bands with broad features (Figure 3). These spectral changes are consistent with previous reports,[18] although the broad Q bands of the radicals beyond 800 nm were not observed due to the lack of a suitable detector in this region. Isosbestic points found during the electrolysis indicate that no detectable intermediates were formed, and the recovery rates were high, greater than 80% for H_2TPBC^- and nearly 90% for H_2TPBC^+.

RR Spectra and Mode Assignments of H_2TPBC^- and H_2TPBC^+. Figure 4 compares 363.8 nm excited RR spectra H_2TPBC and H_2TPBC^-, while isotopomer spectra of the anion radical are collected in Figure 5. For H_2TPBC^+, two excitation lines were used, 363.8 and 406.7 nm, in resonance with the two B bands (Figure 3). Figure 6 displays RR spectra of H_2-TPBC (363.8 nm) and its cation radical (363.8 and 406.7 nm), while 363.8 and 406.7 nm excited RR spectra of H_2TPBC^+ isotopomers are shown in Figures 7 and 8, respectively. In each of these figures, the dotted lines correlate bands of similar vibrational characteristics, as judged from their intensity patterns and isotope shifts. RR spectra of neutral H_2TPBC and its isotopomers in THF and in CH_2Cl_2 are not shown because they

TABLE 1: Selected Skeletal Vibration Frequencies of H_2TPBC and Its Radicals[a]

		$H_2TPBC^{\bullet+}$	H_2TPBC	$H_2TPBC^{\bullet-}$
A_g	ν_{10}	1558	1565[b]	1567
	ν_2	1537	1521	1500
	ν_3	1430		
	ν_4	1356	1367[c]	
	ν_{12}		1297[c]	1295
	ν_1	1222	1226[c]	
	ν_9	1083	1073	1069
	ν_{11}	1022	1027	
	ν_6	980	996	996
B_{1g}	ν_{19}		1560[b]	
	ν_{28}		1421	1425
	ν_{29}	1361	1383	1385
	ν_{27}	1310	1320	1311
	ν_{20}	1250	1266	1241
	ν_{34}	1137		1136

[a] Frequencies of H_2TPBC are the same in THF and CH_2Cl_2; for the radicals, frequencies are measured in a THF solution for the anion radical and in a CH_2Cl_2 solution for the cation radical. [b] Frequencies were obtained with the aid of depolarization measurements to resolve overlapped bands. [c] Data taken from a KBr pellet.

are nearly identical to the KBr pellet reported previously.[10] Vibrational frequencies observed for neutral H_2TPBC and its radicals are listed in Table 1 for comparison. Eigenvectors of selected neutral H_2TPBC vibrations are presented in Figure 9.

The anion spectrum resembles that of H_2TPBC, for which mode assignments are reported and discussed in ref 10. The vibrational frequencies are shifted, and a few additional bands are observed; they are assigned to the skeletal modes ν_{12} and ν_{34} and to symmetric wagging modes of the reduced ring

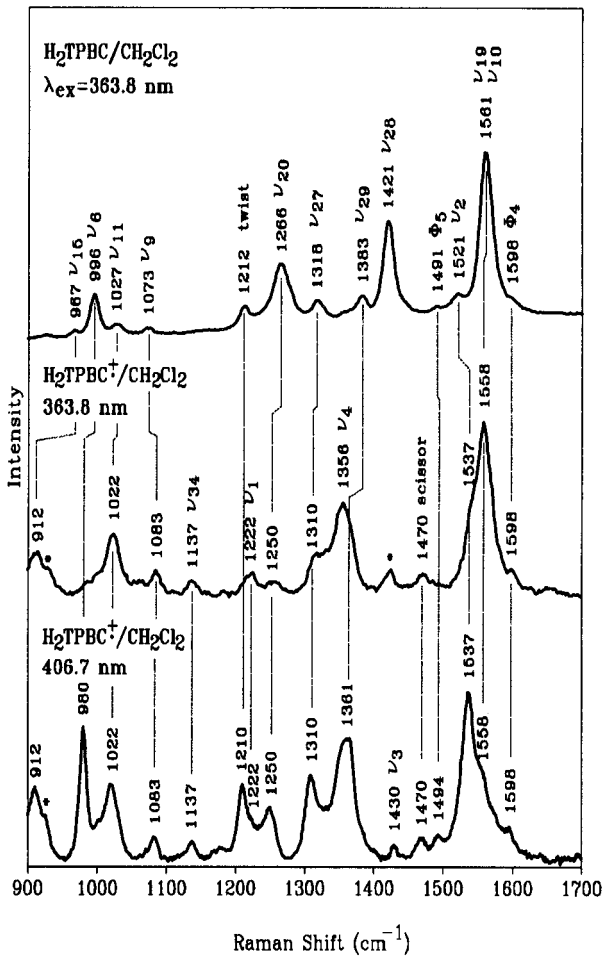

Figure 6. Soret-excited RR spectra of H_2TPBC (363.8 nm) and H_2-TPBC$^+$ (363.8 and 406.7 nm) in CH_2Cl_2/TBAP.

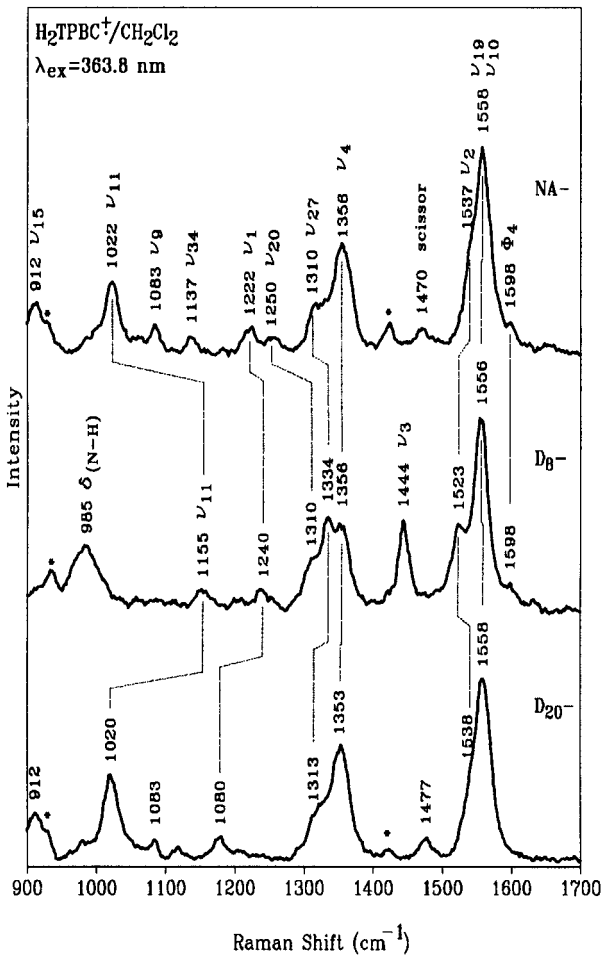

Figure 7. 363.8 nm excited RR spectra of NA-, -d_8, and -d_{20} H_2TPBC$^+$.

methylene groups (Figure 4). ν_{10}, ν_{28}, and ν_{29} are up-shifted for the anion radical, while ν_2, ν_{27}, ν_{20}, and ν_9 are down-shifted, relative to the neutral parent. Among the shifted modes, ν_{10} and ν_2 contain the most valuable information regarding structural changes. ν_{10} is an out-of-phase $C_\alpha-C_m$ bond-stretching mode[10] and is concentrated on the $C_\alpha-C_m$ bonds adjacent to the reduced pyrrole rings, but it also has appreciable contribution from the $C_\alpha-C_m$ bonds adjacent to the pyrrole rings (Figure 9). The slight up-shift (2 cm^{-1}) of ν_{10} implies strengthening of some of the $C_\alpha-C_m$ bonds. The ν_2 mode is a mixture of $C_\alpha-C_m$ and $C_\beta-C_\beta$ bond stretching (Figure 9), and the 21 cm^{-1} down-shift indicates that some of the $C_\alpha-C_m$ bonds and the two $C_\beta-C_\beta$ double bonds are weakened. The ν_4 mode is a marker band for $C_\alpha-C_\beta$ and $C_\alpha-N$ bonds,[10] but it was not enhanced in the 363.8 nm excited RR spectra. Fortunately, the ν_{20}, ν_{27}, and ν_{29} modes observed in the spectra help decipher the $C_\alpha-C_\beta$ and $C_\alpha-N$ bond-order changes. Most of the phenyl vibrations were unshifted as expected, since the aromatic system is not significantly delocalized onto the phenyl groups. However, the ϕ_5 mode down-shifted by 8 cm^{-1}, reflecting a contribution from $C_\beta-C_\beta$ double-bond stretching.[10,19]

For H_2TPBC$^+$, the RR enhancement pattern (Figure 6) is quite different with excitation in the two, well-separated absorption bands in the Soret region. The intensity reversal between ν_{10} and ν_2 is particularly instructive; ν_{10} dominates the 363.8 nm excited spectrum, while ν_2 dominates the 406.7 nm RR spectrum. The eigenvectors (Figure 9) reveal that while both modes involve large $C_\alpha-C_m$ bond displacements, these displacements are parallel to the long axis (y) of conjugation in the π-system for ν_{10}, but parallel to the short axis (x) for ν_2. It is reasonable to suppose that the 356 nm absorption band corresponds to the B_y state, which has a large excited state displacement along ν_{10} (large α_{yy}' tensor element), while the 394 nm absorption band corresponds to the B_x state, which has a large displacement along ν_2. The different enhancement patterns at the two excitation wavelengths help to secure mode assignments with the aid of the isotopomers (Figures 7 and 8). ν_{10} is found to shift down (7 cm^{-1}) relative to the neutral parent, while ν_2 shifts up by 16 cm^{-1}, a pattern opposite of that seen in the radical anion. In addition, vibrational frequency down-shifts are detected for both ν_4 (11 cm^{-1}) and ν_6 (16 cm^{-1}), indicating weakening of the $C_\alpha-C_\beta$ bonds in the pyrrole rings.

TABLE 2: Force Constants Used in Normal Mode Calculation for H_2TPBC and Its Radicals[a]

	$H_2TPBC^{\bullet+}$	H_2TPBC	$H_2TPBC^{\bullet-}$
$\nu(C_\alpha-C_m)$*	6.51	6.90	7.09
$\nu(C_\alpha-C_m)$	6.78	6.50	6.32
$\nu(C_\beta-C_\beta)$	7.51	7.35	7.15
$\nu(C_\alpha-C_\beta)$	4.72	5.02	5.13
$\nu(C_\alpha-N)$*	5.60	5.80	5.43
$\nu(C_\alpha-N)$	5.75	5.70	5.80

[a] The unit for the stretching force constants is mdyn/Å. Asterisks indicate force constants for bonds in or adjacent to the pyrroline rings.

Normal Coordinate Analysis and Molecular Structure. To evaluate the structural changes, we carried out normal coordinate analyses for both the anion and cation radicals, using the force field developed for neutral H_2TPBC.[10] Only bond-stretching force constants were altered (Table 2) to fit the observed frequencies, since we are mainly interested in bond-order changes. The $C_\alpha-C_\beta$ and $C_\beta-C_\beta$ bond-stretching force constants of the pyrroline rings, $\nu(C_\alpha C_\beta)$* and $\nu(C_\beta C_\beta)$*, were not

TABLE 3: Comparison of Observed and Calculated Frequencies and Isotope Shifts of Selected H_2TPBC Anion Radical Vibrations

	obsd				calcd					
mode	NA	$\Delta(^{13}C)$	$\Delta(d_8)$	$\Delta(d_{20})$	NA	$\Delta(^{13}C)$	$\Delta(d_{12})$	$\Delta(d_{20})$	$\Delta(^{15}N)$	assignment (PED, %)
A_g										
ν_{10}	1567	23	5	2	1573	21	7	0	0	58% $\nu(C_\alpha C_m)$*, 13% $\nu(C_\alpha C_m)$, 9% $\nu(C_\beta C_\beta)$, 7% $\nu(C_\alpha C_\beta)$*
ν_2	1500	8	9	4	1510	12	4	5	0	41% $\nu(C_\alpha C_m)$, 10% $\nu(C_1 C_m)$, 7% $\nu(C_\beta C_\beta)$, 7% $\nu(C_\alpha C_\beta)$
ν_3					1443	8	7	−6	0	29% $\delta(HC_\beta H)$*, 16% $\nu(C_\beta C_\beta)$, 15% $\nu(C_\alpha C_m)$*
ν_4					1366	4	11	6	6	24% $\nu(C_\alpha C_\beta)$, 13% $\nu(C_\alpha C_\beta)$*, 10% $\delta(C_m C_\alpha N)$, 9% $\delta(C_\alpha C_m C_\alpha)$, 8% $\delta(C_m C_\alpha N)$*
ν_{12}	1295	10	13	10	1292	0	8	0	11	31% $\nu(C_\alpha N)$*, 31% $\nu(C_\alpha N)$, 8% $\nu(C_\alpha C_\beta)$*, 7% $\nu(C_\alpha C_\beta)$
ν_1			(1245)		1222	3	−5	50	2	30% $\nu(C_1 C_m)$, 15% $\delta(C_p C_p H)$, 11% $\nu(C_\alpha N)$*,6% $\delta(C_1 C_p H)$
ν_9	1069	0		−1	1073	1	307	3	0	38% $\delta(C_\beta C_\beta H)$, 29% $\delta(C_\alpha C_\beta H)$, 8% $\nu(C_\beta C_\beta)$
ν_{11}					1030	3	−123	0	3	20% $\nu(C_\beta C_\beta)$*, 10% $\nu(C_\alpha C_\beta)$, 9% $\delta(C_\beta C_\beta H)$*, 8% $\nu(C_\alpha N)$
ν_6	996	9	17	2	986	2	−2	0	6	25% $\nu(C_\beta C_\beta)$*, 19% $\nu(C_\alpha C_\beta)$, 6% $\nu(C_\alpha C_\beta)$*, 6% $\nu(C_\alpha N)$
B_{1g}										
ν_{19}					1562	31	1	0	0	56% $\nu(C_\alpha C_m)$*, 36% $\nu(C_\alpha C_m)$
ν_{28}	1425	20	9	−3	1420	11	5	−14	3	24% $\nu(C_\alpha C_m)$, 22% $\nu(C_\alpha C_m)$*, 21% $\nu(C_\alpha N)$, 11% $\nu(C_1 C_m)$
ν_{29}	1385	8	161	4	1387	1	75	3	0	47% $\nu(C_\alpha C_\beta)$, 29% $\delta(C_\beta C_\beta H)$, 11% $\delta(C_\alpha C_\beta C_\beta)$, 10% $\delta(C_\alpha C_\beta H)$
ν_{27}	1311	6	−10	4	1318	15	−5	25	12	33% $\nu(C_\alpha N)$, 23% $\nu(C_1 C_m)$, 9% $\delta(C_\alpha NH)$
ν_{20}	1241	6	−50	−14	1245	2	−28	13	10	65% $\nu(C_\alpha N)$*, 11% $\nu(C_\alpha C_\beta)$*, 6% $\nu(C_1 C_m)$
ν_{34}	1136	2		9	1148	1	346	0	1	16% $\delta(C_\beta C_\beta H)$, 16% $\delta(C_\alpha C_\beta H)$, 15% $\nu(C_\alpha C_\beta)$, 12% $\nu(C_\alpha C_\beta)$*

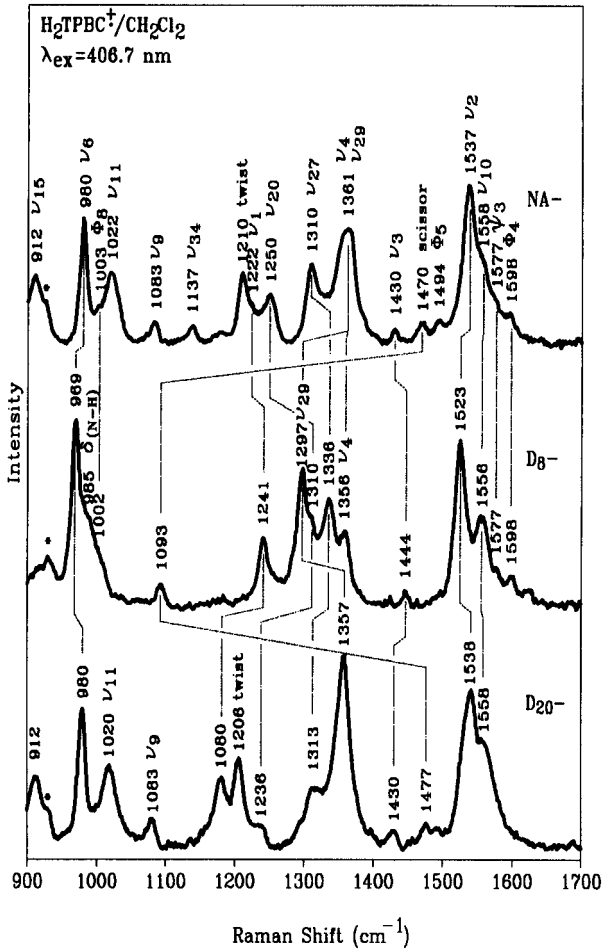

Figure 8. 406.7 nm excited RR spectra of NA-, -d_8, and -d_{20} H_2TPBC$^+$.

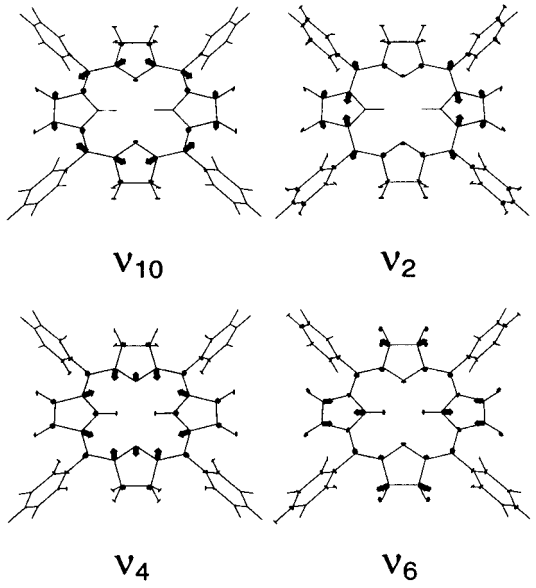

Figure 9. Eigenvector plots of selected vibrational modes for neutral H_2TPBC.

changed because these single bonds are not part of the aromatic system and are not expected to be affected significantly by addition or removal of an electron. Observed and calculated frequencies and isotope shifts are compared in Tables 3 and 4 for the anion and the cation radicals. The frequencies of the vibrational modes, including all those that shift significantly upon radical formation, are well reproduced in the calculation. However, a few modes have discrepant isotope shifts, especially ν_{12} and ν_6 for the anion radical and ν_3 and ν_6 for the cation radical. These discrepancies could probably be remedied by changing some of the interaction force constants, but the data are insufficient to constrain such variation. The phenyl and pyrroline CH_2 modes are not listed because they are not significantly affected by electron addition or removal.

The force constant changes required to fit the radical RR spectra are in gratifying accord with the bonding patterns of the orbitals involved in radical formation. These patterns are diagrammed in Figure 10 for the lowest unoccupied molecular orbital (LUMO) and the highest occupied molecular orbital (HOMO) of an unsubstituted metallobacteriochlorin. The opened and filled circles represent p_z orbitals with opposite phases, and the sizes of these circles are based on the orbital coefficients reported by Sekino and Kobayashi.[20] Also shown in Figure 10 are the force constant changes upon electron addition to the LUMO, or removal from the HOMO (bold, upper right quadrant), as well as the associated bond length changes calculated from the force constant changes via Burgi-Duntz[21] scaling (*italics*, lower left quadrant). We see that force constant decreases (bond length increases) in the anion radical are associated with the antibonding interactions in the LUMO for the $C_\beta-C_\beta$ double bonds, the $C_\alpha-C_m$ bonds adjacent to the pyrrole rings, and the $C_\alpha-N$ bonds in the pyrroline rings. Likewise force constant increases are associated with the

TABLE 4: Comparison of Observed and Calculated Frequencies and Isotope Shifts of Selected H_2TPBC Cation Radical Vibrations

	obsd			calcd				
mode	NA	$\Delta(d_8)$	$\Delta(d_{20})$	NA	$\Delta(d_{12})$	$\Delta(d_{20})$	$\Delta(^{15}N)$	assignment (PED, %)
A_g								
ν_{10}	1558	2	0	1562	6	3	0	41% $\nu(C_\alpha C_m)$, 27% $\nu(C_\alpha C_m)$*, 14% $\nu(C_\beta C_\beta)$
ν_2	1537	14	−1	1530	18	2	0	33% $\nu(C_\beta C_\beta)$, 24% $\nu(C_\alpha C_m)$, 8% $\delta(C_\beta C_\alpha N)$, 7% $\delta(C_\alpha C_\beta H)$, 6% $\nu(C_\alpha C_\beta)$
ν_3	1430	−14	0	1436	−3	−5	1	28% $\delta(HC_\beta H)$*, 28% $\nu(C_\alpha C_m)$*, 9% $\nu(C_\beta C_\beta)$
ν_{14}	1356	0	3	1359	5	6	8	18% $\nu(C_\alpha C_\beta)$*, 17% $\nu(C_\alpha N)$*, 16% $\nu(C_\alpha C_\beta)$,11% $\delta(C_m C_\alpha N)$*, 10% $\delta(C_\alpha N C_\alpha)$*
ν_{12}				1291	11	0	9	29% $\nu(C_\alpha N)$, 26% $\nu(C_\alpha N)$*, 10% $\delta(C_\beta C_\beta H)$*, 9% $\nu(C_\alpha C_\beta)$, 6% $\delta(C_\alpha C_\beta H)$*
ν_1	1222	−18	42	1223	−5	50	2	30% $\nu(C_1 C_m)$, 15% $\delta(C_p C_p H)$, 10% $\nu(C_\alpha N)$*, 6% $\delta(C_1 C_p H)$, 6% $\nu(C_\alpha N)$
ν_9	1083		0	1073	307	2	0	41% $\delta(C_\beta C_\beta H)$, 31% $\delta(C_\alpha C_\beta H)$, 7% $\nu(C_\beta C_\beta)$
ν_{11}	1022	−133	2	1026	−125	3	2	27% $\nu(C_\beta C_\beta)$*, 11% $\delta(C_\beta C_\beta H)$*, 8% $\nu(C_\alpha C_\beta)$, 6% $\delta(C_\beta C_\alpha N)$*
ν_6	980	11	0	977	−3	1	6	25% $\nu(C_\alpha C_\beta)$, 19% $\nu(C_\beta C_\beta)$*, 9% $\nu(C_\alpha N)$
B_{1g}								
ν_{19}				1558	1	2	1	56% $\nu(C_\alpha C_m)$, 31% $\nu(C_\alpha C_m)$*, 7% $\nu(C_\alpha N)$
ν_{28}				1410	5	−16	2	38% $\nu(C_\alpha C_m)$*, 14% $\nu(C_\alpha N)$, 11% $\nu(C_1 C_m)$, 10% $\nu(C_\alpha C_m)$, 8% $\nu(C_\alpha N)$*
ν_{29}	1361	64	4	1362	87	2	0	34% $\nu(C_\alpha C_\beta)$, 26% $\delta(C_\beta C_\beta H)$, 10% $\delta(C_\alpha C_\beta H)$, 9% $\delta(C_\beta C_\beta H)$*, 8% $\delta(C_\alpha C_\beta C_\beta)$
ν_{27}	1310	−26	−3	1316	−4	23	13	37% $\nu(C_\alpha N)$, 22% $\nu(C_1 C_m)$, 10% $\delta(C_\alpha NH)$
ν_{20}	1250	−60	14	1257	−29	14	11	66% $\nu(C_\alpha N)$*, 10% $\nu(C_\alpha C_\beta)$*, 7% $\nu(C_1 C_m)$
ν_{34}	1137			1141	341	0	1	15% $\nu(C_\alpha C_\beta)$*, 15% $\nu(C_\alpha C_\beta)$, 12% $\delta(C_\beta C_\beta H)$, 12% $\delta(C_\alpha C_\beta H)$, 8% $\nu(C_\alpha N)$

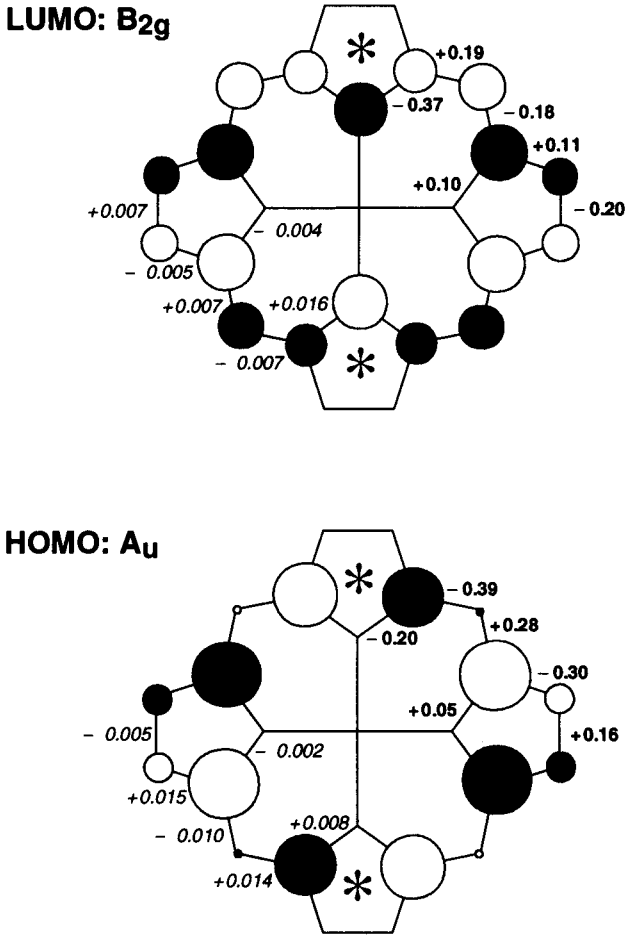

Figure 10. Orbital patterns for the HOMO and LUMO of unsubstituted bacteriochlorin. The radii of the circles are proportional to the coefficients calculated by Sekino and Kobayashi.[20] Asterisks indicate the reduced pyrrole rings. Superimposed on these patterns are the changes in bond-stretching force constant changes (bold), or bond length changes (*italic*, obtained by force constant scaling via method from ref 21) calculated for the H_2TPBC radical anion (LUMO) and cation (HOMO).

bonding interactions of the $C_\alpha-C_m$ bonds adjacent to the pyrroline rings and the $C_\alpha-C_\beta$ bonds in the pyrrole rings. Adding an electron to the LUMO weakens the bonds with the antibonding interactions and strengthens those with bonding interactions. These bonding changes account for the shifts observed in the RR spectra of H_2TPBC^-. For example, the

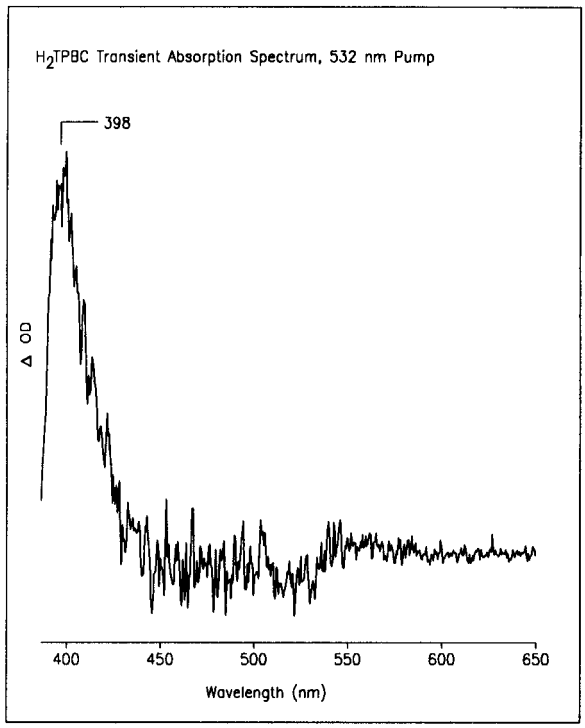

Figure 11. Transient absorption spectrum of H_2TPBC in THF.

pyrroline $C_\alpha-N$ bond weakening produces a large (25 cm^{-1}) down-shift of ν_{20}, which consists mainly (65% of the PED, Table 3) of pyrroline $C_\alpha-N$ bond stretching. Likewise ν_2 shifts down strongly (22 cm^{-1}), reflecting the weakening of the $C_\alpha-C_m$ bonds adjacent to the pyrrole rings (41% of the PED) as well as of the pyrrole $C_\beta-C_\beta$ bonds (7%). At the same time ν_{10} shifts up because of the strengthening of $C_\alpha-C_m$ bonds adjacent to pyrroline rings (58%), but only by 2 cm^{-1} due to the compensating effect of weakening of the $C_\alpha-C_m$ bonds adjacent to the pyrrole ring (13%) and the pyrrole $C_\beta-C_\beta$ bonds (9%).

The bonding changes in the radical cation likewise reflect the orbital pattern of the HOMO (Figure 10). Thus the $C_\beta-C_\beta$ double bonds of the pyrrole rings and the $C_\alpha-C_m$ bonds adjacent to them are subject to antibonding interactions, and removing an electron from the HOMO strengthens these bonds, as reflected in the force constant increases. Likewise, the bonding interactions of the pyrrole $C_\alpha-C_\beta$ bonds and of the $C_\alpha-C_m$ bonds adjacent to pyrroline rings lead to weakening of these bonds in the radical cation and decreases in their force constants.

TABLE 5: Vibrational Frequencies (cm^{-1}) and Isotope Shifts of the H_2TPBC T_1 Excited State

		H_2TPBC (T_1)				
mode	S_0	NA	ΔC_{13}	Δd_{20}	Δd_8	$\Delta S_0 - T_1$
ν_{10}	1565	1537	−12	0	−11	−28
ν_{19}	1560	1590	−37	0	0	+30
ν_{28}	1421	1456	−12	+7	−6	+35
ν_{26}	1358	1358	−4	0		0
ν_4	1367	1326	−4	−3	−14	−39
ν_1	1226	1235	−9	−43	+9	+9
Φ_6	1174[a]	1172	+2		+2	−2
ν_{34}	1134[a]	1118	0			−16
ν_9	1073	1051	−1	−2		−22
ν_6	996	987	+3	+3	−8	−9

[a] Calculated.[10]

TABLE 6: Comparison of Observed and Calculated Frequency (cm^{-1}) Shifts for H_2TPBC Radicals and Excited State

		$(\Delta^{+/0})^a$		$(\Delta^{-/0})^a$		$(\Delta T_1 - S_0)^a$		
mode	S_0	obsd	calcd	obsd	calcd	obsd	calcd[b]	calcd[c]
ν_{10}	1565	−7	−3	+2	+8	−28	−8	−24
ν_{19}	1560	d	−2	d	−5	+30	−4	+17
ν_2	1521	+16	+9	−21	−11	*		
ν_{28}	1421	*		+4	−1	+35	−7	−7
ν_{29}	1383	−22	−21	+2	+4	*		
ν_{26}	1358	*		*		0	−4	−4
ν_4	1367	−11	−8	*		−39	−12	−13
ν_{27}	1320	−10	−4	−9	−2	*		
ν_{12}	1297	*		−2	−5	*		
ν_{20}	1266	−16	−9	−25	−21	*		
ν_1	1226	−4	−3	*		+9	−6	−7
ν_9	1073	+10	0	−4	0	−22	−2	−2
ν_{11}	1027	−5	−1	*		*		
ν_6	996	−16	−19	0	−10	−9	−2	−2

[a] Frequencies in the radical or excited states minus the ground state frequency. [b] Only including bond order changes (the mean of the anion and cation force constants). [c] Including bond order and long-term interaction changes (1,4-($C_\alpha C_m$)($C_\alpha C_m$) and 1,4-($C_\alpha C_m$)*($C_\alpha C_m$)* interaction constants were decreased by 0.1, while the 1,4-($C_\alpha C_m$)($C_\alpha C_m$)* interaction constant was increased by 0.1). [d] The calculated shifts would have ν_{19} overlapped with the strong ν_2 band of the radicals.

Thus ν_2 shifts up 16 cm^{-1} in the radical cation because it is dominated by the stretching of pyrrole $C_\beta - C_\beta$ double bonds (33% of the PED, Table 4) and of $C_\alpha - C_m$ bonds adjacent to the pyrrole rings (24%), while ν_{10} shifts down by a small amount (7 cm^{-1}) because of compensating changes in the two types of $C_\alpha - C_m$ bonds. ν_4 shifts down by 11 cm^{-1} because of weakening of the pyrrole $C_\alpha - C_\beta$ and pyrroline $C_\alpha - N$ bonds.

At a quantitative level, the experimental results are not entirely consistent with the calculated pattern of the HOMO. Thus the p_z coefficient is calculated to be small for the C_m atoms and zero for the pyrroline N atoms, yet the force constant changes of the bonds connecting these atoms are large. Possibly this discrepancy reflects the fact that the calculation is for unsubstituted metallobacteriochlorin, while the experimental results are for the free base of a bacteriochlorin with phenyl substituents at the C_m positions.

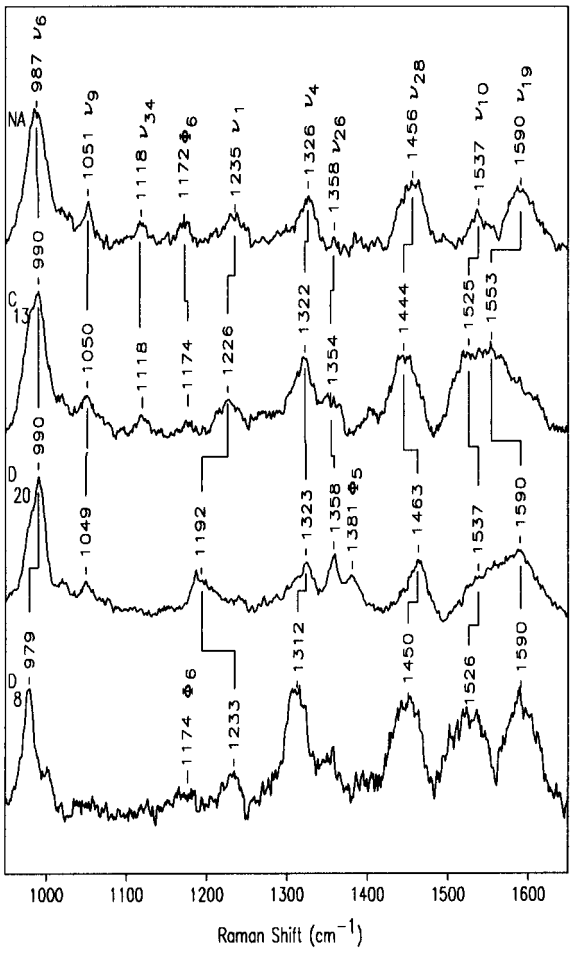

Figure 12. Time-resolved resonance Raman spectra of the T_1 excited state of natural abundance (NA) H_2TPBC and its *meso*-C_{13}, phenyl-d_{20}, and pyrrole-d_8 isotopomers in THF.

T_1 Excited State. The transient absorption spectrum of H_2-TPBC (Figure 11) shows an induced absorption at 398 nm, which is assigned to the $^3(\pi\pi)^*$ T_1 excited state. Time-delay experiments showed this absorption to persist beyond 100 ns, as expected for a triplet state, and the red-shift, relative to the ground state B bands, is consistent with T_1 absorptions for porphyrins[14,22] and chlorins.[23,24] TR[3] spectra (Figure 12) were obtained by pumping at 532 nm, in the Q_x band (Figure 2), and probing at 397 nm near the maximum of the induced absorption. The T_1 enhancement pattern differs from that of the ground state, but the RR bands can be correlated with ground state bands based on similar isotope sensitivities (Table 5).

Three of the four $C_\alpha - C_m$ stretching modes appearing in the ground state RR spectra (ν_2, ν_{10}, ν_{19}, ν_{28}) are seen in the excited state, with similar isotope sensitivities: ν_{19} and ν_{28} shift up (+30 and +35 cm^{-1}), while ν_{10} shifts down (−28 cm^{-1}). ν_2 is not observed. An alternative interpretation would assign ν_{10} and ν_{19} at overlapping positions within the broad 1590 cm^{-1} band, since they have similar isotope sensitivities, and would assign

TABLE 7: Selected Skeletal Vibratonal Frequency (cm^{-1}) Shifts for Radicals of ZnOEP, ZnOEC, and H_2TPBC

	ZnOEP[23b,e,25a]				ZnOEC[26]				H_2TPBC			
mode	S_0	$\Delta^{+/0}$	$\Delta^{-/0}$	$\Delta S_0 - T_1$	S_0	$\Delta^{+/0}$	$\Delta^{-/0}$	$\Delta S_0 - T_1$	S_0	$\Delta^{+/0}$	$\Delta^{-/0}$	$\Delta S_0 - T_1$
ν_{10}	1613	−1	−26		1616	−10	+3	−19	1565	−7	+2	−28
ν_{19}					1565	−29	−1		1560	−2	−5	+17
ν_2	1582	+19	−12	−20	1571	+32		−29	1521	+16	−21	
ν_{11}	1558	+28	−52	+24	1533		+9		1027	−5		
ν_3	1483	−8	−38	−36	1486	+3	+2	−22				
ν_4	1373	−34	−2		1365	−15	−3	−21	1367	−11		−39
ν_9									1073	+10	−4	−22

ν_2 to the 1537 cm^{-1} band. However, this scheme would have all four $C_\alpha-C_m$ bands showing large frequency up-shifts in the excited state, an unlikely situation. The peak at 1326 cm^{-1} is assigned to ν_4 on the basis of its isotope shift pattern, strongly down-shifted from its ground state position, 1367 cm^{-1} (seen with 521 nm excitation[10]). The pyrrole $C_\alpha-C_\beta$ stretching mode, ν_6, down-shifts 8 cm^{-1} from its ground state value, while a larger down-shift, 22 cm^{-1}, is experienced by the $C_\beta C_\beta H$ bending mode, ν_9. Another $C_\beta C_\beta H$ mode, ν_{34}, is assigned to the d_8-sensitive band at 1118 cm^{-1} and is similarly lower (16 cm^{-1}) than the (calculated[10]) ground state frequency. The peak at 1235 cm^{-1} is assigned to the C_m-phenyl stretching mode, ν_9, up-shifted 9 cm^{-1} from its ground state frequency value. Interestingly, the T_1 spectrum contains phenyl modes that are not observed in the ground state or radical spectra: ϕ_6, at 1172 cm^{-1}, and ϕ_5, appearing at 1381 cm^{-1} in the phenyl-d_{20} spectrum; the ϕ_5 frequency should be around 100 cm^{-1} higher in the spectra of the other isotopomers,[10] in which it is likely obscured by the intense ν_{28} feature.

Since the T_1 electronic configuration has an electron in the LUMO and a hole in the HOMO, it might have been expected that the vibrational frequency shifts, relative to the ground state, would be the algebraic sum of the frequency shifts for the radical cation and the radical anion. However, this is clearly not the case (Table 6). Thus ν_{10} and ν_9 experience large down-shifts (-28 and -22 cm^{-1}) in the T_1 state, but much smaller shifts in the radical cation (-7 and $+10$ cm^{-1}) and anion ($+2$ and -4 cm^{-1}).

We investigated the possibility that these discrepancies might arise from a subtle effect of normal mode composition changes by calculating the T_1 vibrational frequencies after averaging the force constant values for the radical cation and anion (Table 2). The frequency shifts, relative to the ground state, were poorly reproduced (Table 6), although the calculations had satisfactorily reproduced the frequency shifts of the radicals. Agreement with observed shifts for ν_{10} and ν_{19} could be improved somewhat by increasing the interaction constant between the $C_\alpha-C_m$ stretches across the bacteriochlorin ring (last column of Table 6). This procedure might be justified if the T_1 state were more delocalized than the ground or radical states. However, the remaining frequency shifts remain quite different from the observed shifts.

We conclude that the structural distortion in the T_1 state is not captured by considering the effects of simply transferring an electron from the HOMO to the LUMO. The large observed frequency shifts imply substantially greater distortion in the T_1 state than in either the radical cation or anion. This inference applies not only to bacteriochlorins but also to chlorins and porphyrins. Table 7 compiles the available frequency shifts for ZnOEP[23b,e,25] (OEP = octaethylporphyrin) and ZnOEC[26] (OEC = octaethylchlorin). As is the case for H_2TPBC, the sums of the radical cation and anion frequency shifts are poor predictors of the T_1 frequency shift. For ZnOEP, these discrepancies might be ascribed to the Jahn−Teller effect, which is operative in the anion[25b] and T_1 state,[23b,e] but not the cation.[25a] However similar discrepancies are seen for ZnOEC, in which no Jahn−Teller effect is possible. Likewise there is no Jahn−Teller effect in H_2TPBC. Thus formation of triplet excited states in tetrapyrrolic macrocycles appears inherently to produce a greater structural distortion than do radical cation and anion formation. The origin of this effect is a challenge to theory, since at the level of MNDO/3 calculations the predicted distortions in the triplet state of Zn porphine were found to be approximately the sum of the radical anion and cation distortions.[27]

Acknowledgment. This work was supported by DOE Grant DE-FG02-93ER-14403.

References and Notes

(1) (a) Deisenhofer, J.; Epp, O.; Miki, K.; Huber, R.; Michel, H. *J. Mol. Biol.* **1984**, *180*, 385−398. (b) Deisenhofer, J.; Epp, O.; Miki, K.; Huber, R.; Michel, H. *Nature* **1985**, *318*, 618−624. (c) Allen, J. P.; Feher, G.; Yeates, T. O.; Komiya, H.; Rees, D. C. *Proc. Natl. Acad. Sci. U.S.A.* **1987**, *84*, 5730−5734; (d) 6162−6166. (e) Yeates, T. O.; Komiya, H.; Rees, D. C.; Allen, J. P.; Feher, G. *Proc. Natl. Acad. Sci. U.S.A.* **1987**, *84*, 6438−6442. (f) Allen, J. P.; Feher, G.; Yeates, T. O.; Komiya, H.; Rees, D. C. *Proc. Natl. Acad. Sci. U.S.A.* **1988**, *85*, 8487−8491. (g) Deisenhofer, J.; Michel, H. *Angew. Chem.* **1989**, *28*, 829−968. (h) McDermott, G.; Prince, S. M.; Freer, A. A.; Hawthornthwaite-Lawless, A. M.; Papiz, M. Z.; Cogdell, R. J.; Isaacs, N. W. *Nature* **1995**, *374*, 517−521.

(2) Scheer, H., Ed. *Chlorophylls*; CRC: Boca Raton, FL, 1991.

(3) For brief introductions, see: (a) Barber, J.; Andersson, B. *Nature* **1994**, *370*, 31−34. (b) Fleming G. R.; van Grondelle R. *Phys. Today* **1994**, *Feb*, 48−55. (c) Norris, J. R.; Schiffer, M. *Chem. Eng. News* **1990**, *July 30*, 22−37.

(4) (a) Lutz, M., Kleo, J. *Biochem. Biophys. Res. Commun.* **1976**, *69*, 711−717. (b) Lutz, M.; Kleo, J. *Biochim. Biophys. Acta* **1979**, *546*, 365−369. (c) Lutz, M.; Hoff, A.; Brehamet, L. *Biochim. Biophys. Acta* **1982**, *679*, 331−341. (d) Cotton, T. M.; Van Duyne *Biochem. Biophys. Res. Commun.* **1978**, *82*, 424−433. (e) Cotton, T. M.; Parks, K. D.; Van Duyne, R. P. *J. Am. Chem. Soc.* **1980**, *102*, 6399−6407. (f) Cotton, T. M.; Van Duyne, R. P. *J. Am. Chem. Soc.* **1981**, *103*, 6020−6026. (g) Callahan, P. M.; Cotton, T. M. *J. Am. Chem. Soc.* **1987**, *109*, 7001−7007. (h) Donohoe, R. J.; Frank, H. A.; Bocian, D. F. *Photochem. Photobiol.* **1988**, *48*, 531−537. (i) Nishizawa, E.; Koyama, Y. *Chem. Phys. Lett.* **1990**, *172*, 317−322. (j) Nishizawa, E.; Koyama, Y. *Chem. Phys. Lett.* **1991**, *176*, 390−394. (k) Peloquin, J. M.; Bylina, E. J.; Youvan, D. C.; Bocian, D. F. *Biochemistry* **1990**, *29*, 8417−8424. (l) Palaniappan, V.; Martin, P. C.; Chynwat, V.; Frank, H. A.; Bocian, D. F. *J. Am. Chem. Soc.* **1993**, *115*, 12035−12049. (m) Diers, J. R.; Bocian, D. F. *J. Phys. Chem.* **1994**, *98*, 12884−12892. (n) Palaniappan, V.; Bocian, D. F. *Biochemistry* **1995**, *34*, 11106−11116.

(5) (a) Donohoe, R. J.; Dyer, R. B; Swanson, B. I.; Violette, C. A.; Frank, H. A.; Bocian, D. F. *J. Am. Chem. Soc.* **1990**, *112*, 6716−6718. (b) Shreve, A. P.; Cherepy, N. J.; Franzen, S.; Boxer, S. G.; Mathies, R. A. *Proc. Natl. Acad. Sci. U.S.A.* **1991**, *88*, 11207−11211. (c) Palaniappan, V.; Aldema, M. A.; Frank, H. A.; Bocian, D. F. *Biochem.* **1992**, *31*, 11050−11058. (d) Feiler, U.; Albouy, D.; Pourcet, C.; Mattioli, T. A.; Lutz, M.; Robert, B. *Biochemistry* **1994**, *33*, 7594−7599. (e) Cherepy, N. J.; Shreve, A. P.; Moore, L. J.; Franzen S.; Boxer, S. G.; Mathies, R. A. *J. Phys. Chem.* **1994**, *98*, 6023−6029. (f) Diers, J. R.; Bocian, D. F. *J. Am. Chem. Soc.* **1995**, *117*, 6629−6630. (g) Palaniappan V.; Schenck, C. C.; Bocian, D. F. *J. Phys. Chem.* **1995**, *99*, 17049−17058. (h) Cherepy N. J.; Holzwarth, A. R.; Mathies, R. A. *Biochemistry* **1995**, *34*, 5288−5293. (i) Diers, J. R.; Zhu, Y.; Blankenship, R. E.; Bocian, D. F. *J. Phys. Chem.* **1996**, *100*, 8573−8579.

(6) (a) Johnson, C. K.; Rubinovitz, R. *Spectrochim. Acta* **1991**, *47A*, 1413−1421. (b) Noguchi, T.; Furukawa, Y.; Tasumi, M. *Spectrochim. Acta* **1991**, *47A*, 1431−1440. (c) Mattioli, T. A.; Hoffmann, A.; Robert, B.; Schrader, B.; Lutz, M. *Biochemistry* **1991**, *30*, 4648−4654. (d) Okada, K.; Nishizawa, E.; Fujimoto, Y.; Koyama, Y.; Muraishi, S.; Ozaki, Y. *Appl. Spectrosc.* **1992**, *46*, 518−523. (e) Wachtveitl, J.; Farchaus, J. W.; Das, R.; Lutz, M.; Robert, B.; Mattioli, T. A. *Biochemistry* **1993**, *32*, 12875−12886. (f) Mattioli, T. A.; Lin, X.; Allen, J. P.; Williams, J. C. *Biochemistry* **1995**, *34*, 6142−6152. (g) Sato, H.; Uehara, K.; Ishii, T.; Ozaki, Y. *Biochemistry* **1995**, *34*, 7854−7860. (h) Sturgis, J. N.; Hagemann, G.; Tadros, M. H.; Robert, B. *Biochemistry* **1995**, *34*, 10519−10524. (i) Sturgis, J. N.; Jirsakova, V.; Reiss-Husson, F.; Cogdell, R. J.; Robert, B. *Biochemistry* **1995**, *34*, 517−523. (j) Feiler, U.; Albouy, D.; Robert, B. Mattioli, T. A. *Biochemistry* **1995**, *34*, 11099−11105. (k) Goldsmith, J. O.; King, B.; Boxer, S. G. *Biochemistry* **1996**, *35*, 2421−2428. (l) Ivancich, A.; Feick, R.; Ertlmaier, A.; Mattioli, T. A. *Biochemistry* **1996**, *35*, 6126−6135. (m) Allen, J. P.; Artz, K.; Lin, X.; Williams, J. C.; Ivancich, A.; Albouy, D.; Mattioli, T. A.; Fetsch, A.; Kuhn, M.; Lubitz, W. *Biochemistry* **1996**, *35*, 6612−6619.

(7) (a) Cotton, T. M.; Parks, K. D.; Van Duyne, P. V. *J. Am. Chem. Soc.* **1980**, *102*, 6399−6407. (b) Diers, J. R.; Bocian, D. F. *J. Phys. Chem.* **1994**, *98*, 12884−12892. (c) Misono, Y.; Limantara, L.; Koyama, Y.; Itoh, K. *J. Phys. Chem.* **1996**, *100*, 2422−2429.

(8) (a) Mäntele, W.; Wollenweber, A.; Rashwan; Heinze, J.; Nabedryk, E.; Berger, G.; Breton, J. *Photochem. Photobiol.* **1988**, *47*, 451−455. (b) Hartwich, G.; Geskes, C.; Scheer, H.; Heinze, J.; Mäntele, W. *J. Am. Chem. Soc.* **1995**, *117*, 7784−7790. (c) Nabedryk, E.; Andrianambinintsoa, S.; Dejonghe, D.; Breton, J. *J. Chem. Phys.* **1995**, *194*, 371−378.

(9) (a) Nishizawa, E.; Koyama, Y. *Chem. Phys. Lett.* **1991**, *176* (3,4), 390−394. (b) Nishizawa, E.; Koyama, Y. *Chem. Phys. Lett.* **1990**, *170* (3,4), 317−322.

(10) Lin, C.-Y.; Spiro, T. G. *J. Phys. Chem. B.* **1997**, *101*, 472−482.

(11) Whitlock, H. W., Jr.; Hanauer, R.; Oester, M. Y.; Bower, B. K. *J. Am. Chem. Soc.* **1969**, *91*, 7485−7489.
(12) Lindsey, J. S.; Schreiman, I. C.; Hsu, H. C.; Kearney, P. C.; Marguerettaz, A. M. *J. Org. Chem.* **1987**, *52*, 827−836.
(13) Czernuszewicz, R. S.; Macor, K. A. *J. Raman Spectrosc.* **1988**, *19*, 553.
(14) Reed, R. A.; Purello, R.; Prendergast, K.: Spiro, T. G. *J. Phys. Chem*. **1991**, *95*, 9720−9727.
(15) Wilson, E. B.; Decius, J. C.; Cross, P. C. *Molecular Vibrations*; McGraw-Hill: New York, 1955.
(16) Barkigia, K. M.; Miura, M.; Thompson, M. A.; Fajer, J. *Inorg. Chem.* **1991**, *30*, 2233−2236.
(17) Mukherjee, A.; Spiro, T. G. *QCPE Bull.* **1995**, *15* (1), Program 656.
(18) (a) Peychal-Heiling, G.; Wilson, G. S. *Anal. Chem.* **1971**, *43*, 550−555. (b) Fajer, J.; Borg, D. C.; Forman, A.; Felton, R. H.; Dolphin, D.; Vegh, L. *Proc. Natl. Acad. Sci. U.S.A.* **1974**, *71*, 994−998.
(19) Li, X.-Y.; Czernuszewicz, R. S.; Kincaid, J. R.; Stein, P.; Spiro, T. G. *J. Phys. Chem.* **1990**, *94*, 31−47.
(20) Sekino, H.; Kobayashi, H. *J. Chem. Phys.* **1987**, *86*, 5045−5052.
(21) Burgi, H.; Dunitz, J. D. *J. Am. Chem. Soc.* **1987**, *109*, 2924−2927.
(22) Rodriguez, J.; Kirmaier, C.: Holten, D. *J. Am. Chem. Soc.* **1989**, *111*, 6500−6510.
(23) (a) de Paula, J. C.; Walter, V. A.; Nutaitis, C.; Lind, J.; Hall, K. *J. Phys. Chem*. **1992**, *96*, 10591−10594. (b) Kumble, R.; Hu, S.; Loppnow, G. R.; Vitols, S. E.; Spiro, T. G. *J. Phys. Chem*. **1993**, *97*, 10521−10523. (c) Bell, S. E.; Al-Obaidi, A. H. R.; Hegarty, M.; Hester, R. E.; McGarvey, J. J. *J. Phys. Chem*. **1993**, *97*, 11599−11602. (d) Sato, S.; Kitagawa, T. *Appl. Phys. B* **1994**, *59*, 415−431. (e) Kreszowski, D. H.; Deinum, G.; Babcock, G. T. *J. Am. Chem. Soc*. **1994**, *116*, 7463−7464. (f) Kumble, R.; Loppnow, G. R.; Hu, S.; Mukherjee, A.; Thompson, M. A.; Spiro, T. G. *J. Phys. Chem.* **1995**, *99*, 5809−5816. (g) Sato, S.; Aoyagi, K.; Haya, T.; Kitagawa, T. *J. Phys. Chem*. **1995**, *99*, 7766−7775. (h) Vitols, S. E.; Kumble, R.; Blackwood, M. E., Jr.; Roman, J. S.; Spiro, T. G. *J. Phys. Chem.* **1996**, *100*, 4180−4187.
(24) de Paula, J. C.; Walters, V. A.; Jackson, B. A. Cardozo, K. *J. Phys. Chem.* **1995**, *99*, 4373−4379.
(25) (a) Oertling, W. A.; Salehi, A.; Chung, Y. C.; Leroi, G. E.; Chang, C. K.; Babcock, G. T. *J. Phys. Chem*. **1987**, *91*, 5887−5898. (b) Hu, S.; Lin, C.-Y.; Blackwood, M. E., Jr.; Mukherjee, A.; Spiro, T. G. *J. Phys. Chem.* **1995**, *99*, 9694−9701.
(26) (a) Blackwood, M. E., Jr.; Kumble, R.; Spiro, T. G. *J. Phys. Chem*. **1996**, *100*, 18037−18041. (b) Blackwood, M. E., Jr.; Spiro, T. G. In preparation.
(27) Prendergast, K.; Spiro, T. G. *J. Am. Chem. Soc.* **1991**, *95*, 9728−9736.